Supporting Information

Dupuy et al. 10.1073/pnas.0906322107

SI Text

A Simple Biomechanical Model for *Coleochaete*. A simple analytical model (Fig. S1) enables an explicit link between the cell-wall viscosity coefficient and the radial expansion rate of the specimens (Eq. **1**). The viscosity coefficient can in turn be simply estimated from experimental growth curve (Fig. 1*B*) using least square techniques and be used to perform finite element computations on more complex structures.

Kinematics. Cell expansion and division concern exclusively the first layer of cells at the periphery of the thallus. Cell size (radial *lr* and tangential *lt*) in this layer is assumed to remain constant. Cell expansion is assumed to be linear in boundary cells and null for interior cell. Therefore, velocity field can easily be expressed as a function of the rate of radial expansion $\dot{R}$ and the radial position r

$$\begin{cases} \mathbf{v} = \dot{R}\left(\dfrac{r-R+l_r}{l_r}\right)\mathbf{e}_r; r \in [R-l_r, R] \\ \mathbf{v} = 0; r < R-l_r \end{cases} \quad [S1]$$

The strain rates on $[R-l_r, R]$ in the radial and tangential directions are $\dot{\varepsilon}_t = \dot{R}/R$ and $\dot{\varepsilon}_r = \dot{R}/l_r$.

Tensile forces in cell walls. Strain in cell walls is therefore constant and depends only on orientation. Therefore, assuming a perfect viscous material property, it is possible to relate expansion rate of the specimen to tensile forces in cell walls:

$$\begin{cases} F_t = \mu S_t \dot{R}/R \\ F_r = \mu S_r \dot{R}/l_r \end{cases} \quad [S2]$$

where F_r and F_t are the tensile forces in radial and tangential cell walls, μ is the viscosity coefficient ($Pa{\cdot}s$) of the wall, and S_t and S_r are cell wall cross-sections in tangential and radial direction. If radial and tangential cell walls have the same width e, S_t and S_r are equal to he. Cell wall cross-section is assumed to remain constant throughout deformation.

Expansion of the thallus. If the expansion is slow, it is possible to neglect the forces of inertia, and the forces present in cell walls must equal the force applied by turgor on cell walls. Projecting the equilibrium of forces on half the specimen on the vertical axis as shown in Fig. S1*C*, it follows that:

$$2\mu S_t \dot{R}/R + \int_0^{\pi} \mu S_r \dot{R}/l_r \sin(\theta)/l_t R d\theta = \int_0^{\pi} (P-P_0) h \sin(\theta) R d\theta, \quad [S3]$$

where h is the height of cells in the z direction. From the equilibrium of forces acting on cell walls, it is possible to derive an expression of the radial growth of the system:

$$\dot{R} = \frac{(P-P_0)\, hRl_r l_t}{(S_t l_r l_t/R + S_r R)\, \mu}. \quad [S4]$$

When the radius becomes large relative to the dimensions of the cell, and if it is assumed that radial and tangential cell wall have the same width e (S_t and S_r are equal to he), the expression of μ reduces to $\mu \approx P.l_r l_t/(e\dot{R})$ and can easily be used for the estimation of the viscosity coefficient from experimental data.

Computational Model for Plant Morphogenesis. In this section, we outline the application of the finite element method for modeling cellular growth. To obtain a more detailed introduction on the finite element method, we encourage the reader to refer to classical structural mechanics textbooks (1).

In the finite element model, cell walls are represented as a network of 2D beams. Each beam is defined by two nodes denoted $X_i = (X_{i1}, X_{i2})$ (Fig. S2*D*). Turgor pressure inside the cells is converted into external punctual forces applied at each node of the structure. These punctual forces equal half of the pressure applied on the incident side walls (Fig. S2*A*).

This beam structure deforms in reaction to the application of these external forces, and the finite element method provides a theoretical basis for determining how single-element behavior integrates in the global behavior of the structure. The key component for describing the behavior of mechanical elements is the stiffness matrix K. This matrix is such that the multiplication of K by the vector of displacements at the nodes of the element equals the external forces required to obtain that displacement. If it is assumed that nodes can only transfer axial forces then we have at a given time step:

$$\begin{pmatrix} P_{i1} \\ P_{i2} \\ P_{(i+1)1} \\ P_{(i+1)2} \end{pmatrix} = \begin{bmatrix} \mu dtS/L & 0 & -\mu dtS/L & 0 \\ 0 & 0 & 0 & 0 \\ -\mu dtS/L & 0 & \mu dtS/L & 0 \\ 0 & 0 & 0 & 0 \end{bmatrix} \begin{pmatrix} V_{i1} \\ V_{i2} \\ V_{(i+1)1} \\ V_{(i+1)2} \end{pmatrix} \quad [S5]$$

The global behavior of the whole structure is obtained by "assembling" the global stiffness matrix of the whole structure:

$$\begin{pmatrix} \dots \\ P_{i1} \\ P_{i2} \\ P_{(i+1)1} \\ P_{(i+1)2} \\ \dots \end{pmatrix} = \begin{bmatrix} \dots & \dots & \dots & \dots & \dots & \dots \\ \dots & \mu dtS/L & 0 & -\mu dtS/L & 0 & \dots \\ \dots & 0 & 0 & 0 & 0 & \dots \\ \dots & -\mu dtS/L & 0 & \mu dtS/L & 0 & \dots \\ \dots & 0 & 0 & 0 & 0 & \dots \\ \dots & \dots & \dots & \dots & \dots & \dots \end{bmatrix} \begin{pmatrix} \dots \\ V_{i1} \\ V_{i2} \\ V_{(i+1)1} \\ V_{(i+1)2} \\ \dots \end{pmatrix} \quad [S6]$$

To account for bending forces and rotations, which include 3 degrees of freedom per node (longitudinal, transversal, and rotational displacement), the following element tangential stiffness K^i matrix is used:

$$K^i = \mu dt \begin{bmatrix} S/L & 0 & 0 & -S/L & 0 & 0 \\ 0 & 12I/L^3 & 6I/L^2 & 0 & 0 & 0 \\ 0 & 6I/L^2 & 4I/L & 0 & 0 & 0 \\ -S/L & 0 & 0 & S/L & 0 & 0 \\ 0 & 0 & 0 & 0 & 12I/L^3 & 6I/L^2 \\ 0 & 0 & 0 & 0 & 6I/L^2 & 4I/L \end{bmatrix} \quad [S7]$$

The next step of the analysis consists of finding the displacements V_i at the nodes of the structure when the forces at the nodes are known (Fig. S2*C*). This is done by finding the solution of the problem in Eq. **S6**, for which various numerical algorithms exist. Once the displacement at the finite set of nodes of the structure has been found, it is possible to determine the continuous de-

formation of the beam using Hermite cubic polynomials. Internal stresses within the structure can be computed from the displacements V_i using the stress-strain relationship (Fig. S2*D*). Finally, the numerical solution discussed above is verified against the analytical solution presented in Eq. **S4** (Fig. S2*E*). More details on the Euler Bernoulli method can be found in classical textbooks on the finite element method (see main text).

Cell Division Model. The biomechanical model for cell growth is coupled to a cell division model based on the sensing of cell shape. The algorithm follows four steps:

1. In the first step, cells are initiated (either at the start of the simulation or when a cell division occurs) with an intrinsic limit size. This limit cell area is drawn randomly according to a uniform distribution (377-856 μm^2; cf. Fig. 2) or normally distributed (mean 610 μm^2, SD 110 μm^2).
2. Cell shape is calculated: the tangential direction is determined as the vector parallel to the boundary wall, and the radial direction is the cross-product of the tangential vector with the z vector. Cell shape (l_r and l_t) is computed as the projection of the cell on these two axes. The cell center is calculated as the center of mass of the cell area.
3. Each cell is tested for cell division: the cell area is compared with the intrinsic limit area. If the limit is reached, division is computed according to the model in Eq. **2** and using parameters derived from cell division data (a = 0.85, s = 0.055). The cell division is asymmetric: this appears both from the fact that the limit between anticlinal and periclinal divisions is not symmetric in Fig. 2, and the measurement of cell sizes at the border and inside the thallus. We chose a 2/3:1/3 ratio because it is required for border cells to have the same size as interior cells.
4. The next growth increment is computed, and steps 2 and 3 are reiterated.

To compare the distribution of cell size at division with the result of the simulations, we have transformed the variables describing the cell shape to remove the correlations that exist between l_r and l_t (Fig. 2) ($R^2 = 0.25$). We chose the cross-section area A ($l_r \times l_t$) and the ratio between radial and tangential size R (l_t/l_r) as random variables to perform the comparisons. After transformation, A and R had weak correlations ($R^2 = 0.04$), and we have used quantile–quantile plots (Q–Q plots) to assess the differences between experimental and simulated A and R distributions independently (Fig. S3).

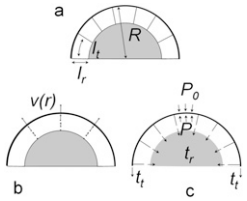

Fig. S1. The geometrical assumptions (*A*) of the analytical model consist of a perfectly circular colony of radius R, whose cells show constant radial l_r and tangential l_t length. The kinematics hypotheses (*B*) assume that velocity field is only in the radial direction. Interior cells ($r < R - l_r$) are fixed, and a linear increase (i.e., constant strain rate) in the velocity field is observed for boundary cells until $r = R$. As a consequence, the velocity field in the whole system is a function of cell radial length l_r and expansion rate dR/dt. The forces (*C*) which put the system in equilibrium, neglecting dynamic effects, are pressure inside (P) and outside (P_0) the cell, tensile forces in walls in the radial direction (t_r), and tensile forces in walls in the tangential direction (t_t).

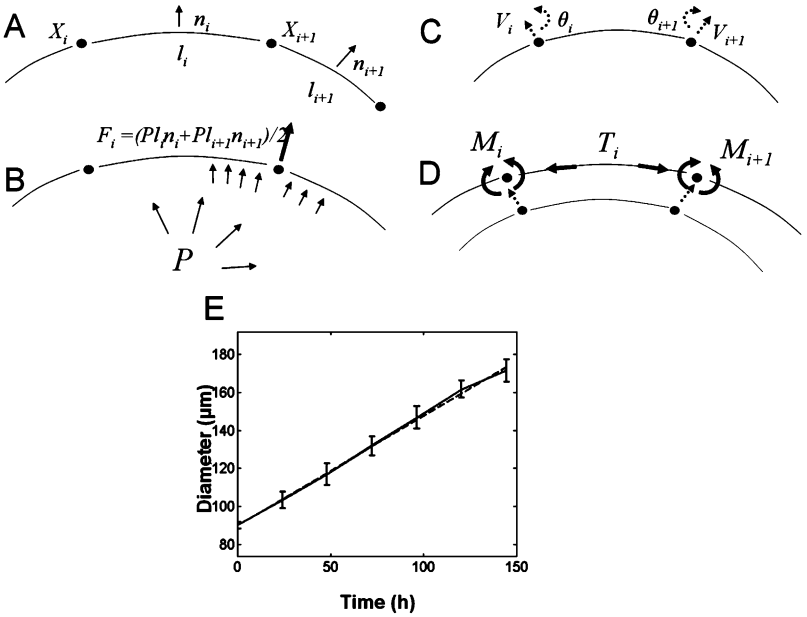

Fig. S2. Principal steps for the finite element analysis of cellular structures. (*A*) The structure is decomposed into beam elements defined by pairs of nodes (X_i,X_j). The mechanical behavior of individual beam elements is defined by their length l_i, the properties of their sections, and the material properties (e.g., viscosity). (*B*) Turgor pressure is transcribed into punctual forces on the node of the structure. (*C*) Translational and rotational displacements are the unknowns of the problem. The stiffness matrix of the structure (e.g., Eq. **S6**) encodes the relationship between the displacements and the forces required to deform it accordingly. A numerical algorithm, e.g., scaled gradient conjugate, is used to find the displacements that correspond to the forces applied at the nodes of the structure. (*D*) Internal stresses and forces are computed a posteriori using the material properties (stress-strain relationship). (*E*) The numerical solution (solid line) is verified against the analytical model (dashed line) described in Eq. **S4**. Error bars are ±SE from three different simulations where a measure of the radius is obtained for each cell on the border of the thallus.

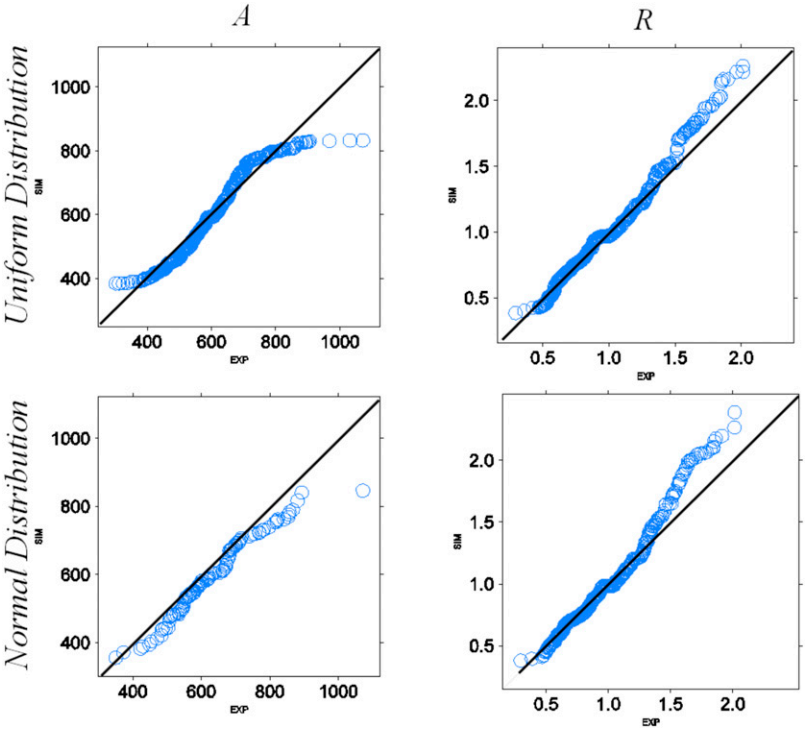

Fig. S3. Q–Q plots for the comparison of measured and simulated cell size at division. Comparisons are for the two transformed variables $A = l_r \times l_t$, and $R = l_r/l_t$ when limit cell area is drawn from a uniform distribution and when limit cell area is drawn from a normal distribution.

1. Coen E, Rolland-Lagan A-G, Matthews M, Bangham AJ, Prusinkiewicz P (2004) The genetics of geometry. *Proc Natl Acad Sci USA* 101:4728–4735.